Direct Detection of Galactic Halo Dark Matter

B. R. Oppenheimer,[1]* N. C. Hambly,[2] A. P. Digby,[2]
S. T. Hodgkin,[3] D. Saumon[4]

The Milky Way galaxy contains a large, spherical component which is believed to harbor a substantial amount of unseen matter. Recent observations indirectly suggest that as much as half of this "dark matter" may be in the form of old, very cool white dwarfs, the remnants of an ancient population of stars as old as the galaxy itself. We conducted a survey to find faint, cool white dwarfs with large space velocities, indicative of their membership in the galaxy's spherical halo component. The survey reveals a substantial, directly observed population of old white dwarfs, too faint to be seen in previous surveys. This newly discovered population accounts for at least 2 percent of the halo dark matter. It provides a natural explanation for the indirect observations, and represents a direct detection of galactic halo dark matter.

Dark matter in the spherical halo of the Milky Way galaxy has been inferred because the gravitational field due to the known distribution of luminous matter, primarily stars, cannot explain the observed rotational characteristics of the galaxy's spiral disk. A substantial portion of this unseen matter may be old, very cool white dwarfs (*1–4*). A white dwarf is the extremely dense end-state in the evolution of stars with masses less than about eight times the mass of the sun ($M_\odot$). Once a star becomes a white dwarf, it no longer produces energy through nuclear fusion, and therefore cools and fades. The first four examples of ultracool white dwarfs, whose temperatures are below 4000 K, were identified only in the past 2 years (*2, 3, 5–7*), principally because they were too faint to detect in previous surveys. They have spectral energy distributions that differ dramatically from those of the hotter white dwarfs, consistent with white dwarf atmosphere models (*8–10*). The difference is due to the formation of H_2 molecules in white dwarf atmospheres with effective temperatures below ~4500 K. Although H_2 molecules are symmetric and thus have no dipole moment, in the high densities of white dwarf atmospheres, collisions between the molecules are common. These collisions induce momentary dipole moments, which produce opacity at wavelengths longer than 0.6 μm (*11*). We conducted a survey to search for nearby, high-proper-motion white dwarfs that could be halo members and might exhibit this opacity. Regardless of their spectral appearance, nearby halo stars can be distinguished from disk stars by their space motion, because the two populations possess different kinematic properties.

Observations. Our survey used digitized, photographic plates in the *R59F* and B_J passbands from the SuperCOSMOS Sky Survey (*12–14*). *R59F* and B_J roughly correspond to optical wavelengths of 0.59 and 0.45 μm, respectively. We searched for objects with proper motions, μ, between 0.33 and 10.00″ year^{-1} as faint as $R59F = 19.8$, using plates near the South Galactic Cap (SGC) at three epochs in each field. The SGC plates comprise 196 fields (*15*). The nonoverlapping area of each field is 25 square degrees. Hence, the area of our survey is 4900 square degrees, or about 12% of the sky. Because of image blending problems and large halos of scattered light around bright stars, the actual area surveyed is 4165 square degrees, or 10% of the sky. This is several times larger than the areas searched in two previous surveys (*3, 16*). At the very faint end of our sample, we found many objects not included in the Luyten catalogs of proper motion stars (*17*), primarily because Luyten's survey in the Southern Hemisphere did not attempt to find objects as faint as those we have found. These previously undetected stars are the principal members of our sample of halo white dwarfs.

We used the technique of reduced proper motion (RPM) (*18, 19*) to identify white dwarfs by their subluminosity in comparison to main-sequence stars and their high intrinsic space motions. RPM is defined as $H_R = R59F + 5 \log \mu + 5$, and is an estimate of the absolute magnitude based on the proper motion, μ, in arc seconds per year. We selected all 126 objects in the RPM diagram (Fig. 1) having either $H_R > 22.5$ or lying in the subluminous regions as potential halo white dwarfs. Sixty-three of these were previously cataloged (*12, 20*). Of these 63 known, high-proper-motion stars, 29 had no published spectroscopic follow-up. This yielded an observing list of 92 stars for follow-up, including 63 new discoveries.

Over 4 nights (11 to 14 October 2000) at the Cerro Tololo Inter American Observatory's V. M. Blanco 4-m Telescope, we obtained spectra in the wavelength range 0.48 to 0.98 μm for 69 of the 92 candidates (filled symbols in Fig. 1). We inspected the spectra within minutes of collecting the data, so we were able to discern by the middle of the second night which types of objects populated which parts of the RPM diagram (Fig. 1). For example, as expected, we found only white dwarfs with Hα features on the far left of the subluminous sequence. Dwarf and subdwarf M-type stars are restricted to the right, which is also the bottom of the main sequence. We concentrated our observing resources on the cool objects, which occupy the lower part of the subluminous sequence. Of the 69 candidate objects observed, 16 are M-dwarfs or M-subdwarfs, two are hot He white dwarfs, 13 are white dwarfs with Hα features, and 38 are new cool white dwarfs (Fig. 2A), a few of which are probably cooler than WD0346+246, the prototypical

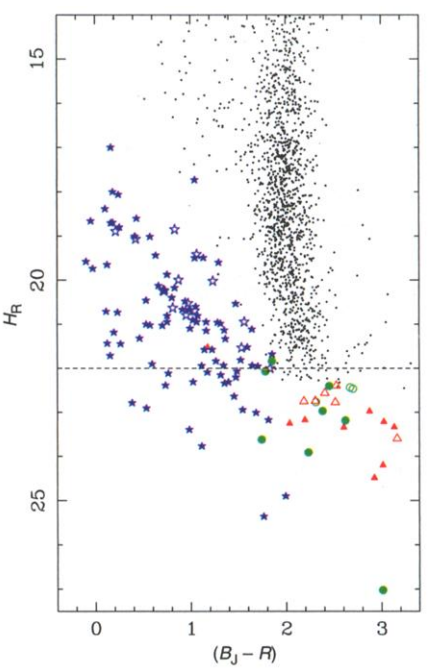

Fig. 1. Reduced proper motion diagram. All low-luminosity, proper-motion objects in our survey are shown. The main sequence extends from the top-center downward. The subluminous sequence to the left and below is the white dwarf sequence. Blue, filled stars indicate white dwarfs confirmed with our spectroscopy or previously known to be white dwarfs. Open stars are objects we have not yet observed spectroscopically but presume to be white dwarfs on the basis of their location in this diagram. Filled, red triangles are M-dwarfs and filled, green circles are subdwarfs for which we obtained spectra. Open triangles and open circles are suspected M-type dwarf or subdwarf stars, respectively, which we did not observe. The dashed line indicates the value of H_R below which the Luyten catalogs (*17*) contain very few objects.

[1]Astronomy Department, University of California-Berkeley, Berkeley, CA 94720–3411, USA. [2]Institute for Astronomy, University of Edinburgh, Royal Observatory, Blackford Hill, Edinburgh, EH9 3HJ, UK. [3]Institute of Astronomy, Cambridge University, Madingley Road, Cambridge, CB3 0HA, UK. [4]Department of Physics and Astronomy, Vanderbilt University, Nashville, TN 37235, USA.

*To whom correspondence should be addressed. E-mail: bro@astron.berkeley.edu

ultracool white dwarf, which exhibits the H_2 opacity (*2, 7, 21, 22*).

Two of the 38 new cool white dwarfs have unusual spectra (Fig. 2B). One, LHS 1402, has a spectrum very similar to those of the peculiar stars LHS 3250 (*5, 7*) and SDSS 1337+00 (*6*), but with a steeper slope toward longer wavelengths, suggesting a cooler temperature. The other object, WD2356-209, possesses a bizarre spectrum, incomparable to any other known object. We reanalyzed the data on this object several times and found no evidence for residual instrumental effects.

White dwarfs in the galactic halo. The 38 cool white dwarfs in our sample show no spectral lines (e.g., Fig. 2A), preventing determination of their radial velocities. Nevertheless, we can estimate their space motions from the tangential velocity, $v_{tan} = \mu d$, where μ is the proper motion and d is the distance between each star and Earth. To estimate distances, we used a photometric parallax relation derived from a linear least-squares fit to the cool white dwarf sample of Bergeron, Ruiz, and Leggett (*23*), supplemented by the ultracool WD0346+246, yielding the absolute magnitude in the B_J filter, $M_{B_J} = 12.73 + 2.58(B_J - R59F)$. Our calculations of the spectra of very cool white dwarfs also show a linear relation between M_{B_J} and $B_J - R59F$. The color turnoff in $B_J - R59F$ due to collision-induced absorption by H_2 molecules in the pure hydrogen atmospheres becomes apparent in $B_J - R59F$ only at effective temperatures below 2500 K. The distances derived by this method are listed in Table 1. The scatter of the data around the least-squares fit results in a 20% uncertainty in our distance estimates. For LHS 147 and LHS 542, the only stars in Table 1 with measured distances (*16, 24*), our estimates and the measured distances agree within 1 and 20%, respectively.

In order to use the velocities of the stars as an indicator of membership in the galactic halo, we transformed v_{tan} into the components U, V, and W, in galactic coordinates. U is radial away from the galactic center, V is in the direction of rotation, whereas W is perpendicular to the galactic disk. The calculations used to derive these velocities take into account the deviation of the velocity of the sun with respect to the average velocity of nearby stars in the Galactic disk. Because our survey was centered around the SGC, our observations are most sensitive to the U and V velocities (Fig. 3). Therefore, the most reasonable assumption is that W is zero for all of our stars. Zero is also the average value of W for all stars in the Milky Way. The point where U, V, and W are all equal to zero defines the so-called "local standard of rest," a frame of reference which is rotating in the disk about the galactic center at the average rotation velocity of the disk near the sun. Halo objects, because they have an isotropic velocity distribution with little or no overall rotation, should lag behind the local standard of rest with a distribution centered near $V = -220$ km s^{-1}, because the local standard of rest orbits the galaxy at 220 km s^{-1} (*25*).

Our survey contains 38 stars that unambiguously possess halo kinematics (Fig. 3). We selected a sample of halo stars by accepting all objects whose velocities exceed the $2\sigma = 94$ km s^{-1} velocity dispersion for the old disk stars (*25*). Our velocity cut excludes some halo stars with lower velocities, but permits only minimal contamination of the sample by disk stars. By choosing stars above $2\sigma = 94$ km s^{-1}, we excluded 95% of the disk stars.

Furthermore, if a portion of our sample contains binary stars [the fraction of white dwarfs that are in white dwarf–white dwarf pairs is between 2 and 20% (*26*)], we expect that the velocity distribution of halo stars (Fig. 3) will be biased toward the point $(V,U) = (0,0)$. This is because we assumed that all of the stars are solitary in our estimate of distance. For those that are actually binary, we underestimated the intrinsic luminosity by, at most, a factor of 2 and the distance by a factor of $\sqrt{2}$. Therefore, the values of U and V are underestimated by the same factor of $\sqrt{2}$. This bias is apparent in our sample (Fig. 3), implying that while we may have included a few disk stars in our sample, we may also have excluded a few binary halo stars.

Because we searched for stars having $\mu > 0.33''$ year^{-1}, there is a lack of stars with very low space motions. Furthermore, because of large differences in the epochs of the plates, an object with a proper motion $>3''$ year^{-1} will have a displacement of at least $30''$ between the plates. This compromises the detection of objects with extremely high space motions: even though we searched for objects having annual motions of up to $10''$, our survey probably had less than a 10% chance of finding very faint stars moving by $3''$ year^{-1} or more. These biases against stars with very low and very high space motions result in the dearth of points within 50 km s^{-1} of the point $(U,V) = (0,0)$ and the paucity of points at the extreme left of the UV velocity diagram (Fig. 3). Therefore, we underestimated the numbers of halo white dwarfs, and we measured a lower limit to the space density of these objects.

The subset of objects with velocities outside the 2σ velocity dispersion of the old disk stars (Fig. 3) contains 24 cool white dwarfs and 14 white dwarfs with Hα features (Table 1). An initial estimate of the space density of these objects is obtained using only the 12 coolest white dwarfs, whose absolute magnitudes, M_{R59F}, are approximately 16. With the survey depth of 19.8 and the survey area, a rough volume is computed yielding a space density of 2×10^{-4} pc^{-3}, or $1.2 \times 10^{-4}\ M_\odot$ pc^{-3}.

To obtain a more precise estimate of the

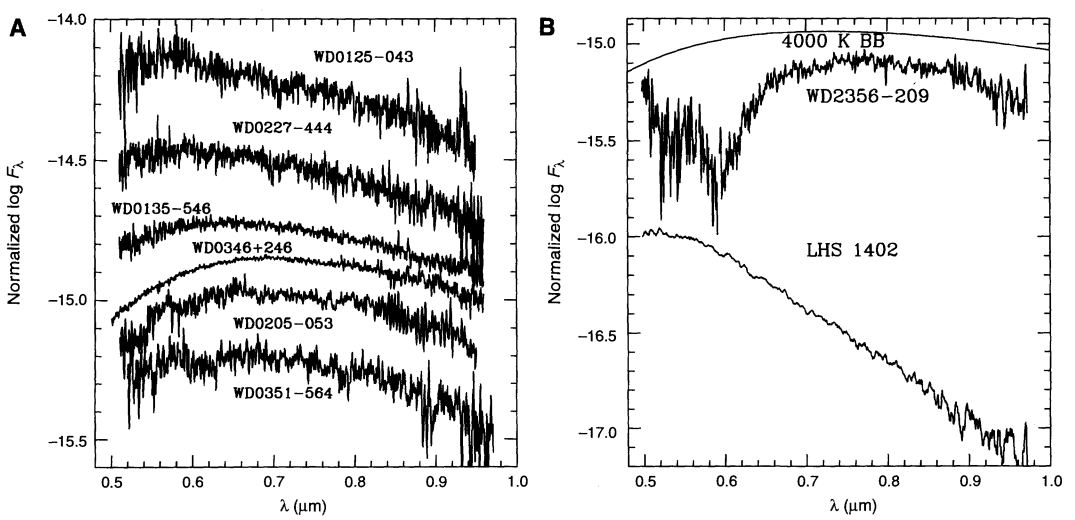

Fig. 2. Selected spectra of new cool white dwarfs. WD0346+246 is included for comparison. **(A)** contains five spectra representative of the set of 24 cool halo white dwarfs (without Hα features) such that the full range of spectral shapes in this set is presented. The spectra, normalized and shifted vertically to facilitate comparison, are ordered according to the sequence in Fig. 4, from top down in order of increasing $B_J - R59F$. This sequence roughly corresponds to decreasing temperature. **(B)** shows the odd spectrum of WD2356-209, which has no analogs, the spectrum of LHS 1402, which seems to be a cooler analog of LHS 3250 and SDSS 1337+00, and a 4000 K blackbody (BB) spectrum at the top. Object names used in Table 1 are indicated. None of the fine features are real.

Table 1. Candidate Halo White Dwarfs. WD names are new discoveries; otherwise, Luyten LHS or LP names are given; J0014-3937 was discovered by Scholz *et al.* (*20*), who classify this object as "cool, no Hα," and F351-50 was discovered by Ibata *et al.* (*3*). The tangential velocity, v_{tan}(est) in km s^{-1}, is an estimate based on photometric parallax. Distances are estimates based on a color-magnitude relation (see text). Star positions are given in right ascension (RA) and declination (Dec.) at the equinox and epoch of 2000.00. The proper motion, μ, and position angle, PA, are given in " year^{-1} and degrees, respectively. The photometric measurements in B_J, *R59F*, and I_N are given in magnitudes, with uncertainties of ±0.1 mag on average. The distance is in parsecs from the sun.

Star name	RA and Dec. (Equinox and epoch 2000.00)		μ (" year^{-1})	PA (degrees)	B_J (mag)	(B_J − *R59F*) (mag)	(*R59F* − I_N) (mag)	v_{tan}(est) (km s^{-1})	Dist. (pc)
F351-50	00:45:19.695	−33:29:29.46	2.490 ± 0.069	128.0	20.13	1.76	0.81	440	37
WD0153-014*	01:53:51.454	−01:23:40.76	0.395 ± 0.010	170.8	18.87	0.15	0.0†	265	141
LHS 542	23:19:09.518	−06:12:49.92	1.695 ± 0.029	200.7	18.72	1.11	0.70	339	42
WD0351-564	03:51:09.376	−56:27:07.12	1.085 ± 0.027	165.8	21.70	1.98	0.5†	305	59
LHS 147*	01:48:09.120	−17:12:14.08	1.095 ± 0.028	186.6	17.96	0.38	0.30	367	71
WD2326-272	23:26:10.718	−27:14:46.68	0.603 ± 0.057	99.5	20.46	0.99	0.3†	310	108
WD0135-039*	01:35:33.685	−03:57:17.90	0.503 ± 0.020	111.0	19.92	0.53	0.34	348	146
LHS 4042*	23:54:35.034	−32:21:19.44	0.427 ± 0.020	95.7	17.66	0.11	0.24	172	85
WD2356-209	23:56:45.091	−20:54:49.31	0.391 ± 0.044	237.3	21.12	1.45	0.61	158	85
WD0227-444	02:27:29.562	−44:23:08.64	0.344 ± 0.021	129.0	20.40	1.27	0.51	124	76
J0014-3937	00:13:47.465	−39:37:24.00	0.739 ± 0.024	198.5	19.35	1.39	0.70	142	40
LHS 4033*	23:52:31.941	−02:53:11.76	0.723 ± 0.056	62.8	17.40	0.26	0.05	216	63
LP 586-51*	01:02:07.181	−00:33:01.82	0.417 ± 0.105	128.7	18.44	0.12	−0.16	238	120
WD2242-197	22:41:44.252	−19:40:41.41	0.367 ± 0.040	76.5	20.04	0.76	0.34	204	117
WD0205-053	02:05:11.620	−05:17:54.33	1.051 ± 0.025	67.6	19.57	1.69	0.80	156	31
WD0100-645*	01:00:50.394	−64:29:11.21	0.560 ± 0.048	70.9	17.98	0.70	0.30	130	49
WD0125-043	01:25:05.884	−04:17:02.56	0.409 ± 0.135	80.6	20.26	1.02	0.32	185	95
WD2346-478*	23:46:02.857	−47:51:01.92	0.533 ± 0.050	219.6	18.44	0.99	0.42	108	43
LHS 1447	02:48:13.182	−30:01:32.40	0.550 ± 0.055	51.4	18.78	0.59	0.18	210	80
WD0300-044	03:00:23.644	−04:25:24.78	0.390 ± 0.026	135.8	20.15	0.73	0.1†	237	128
WD0123-278	01:23:03.784	−27:48:14.59	0.352 ± 0.040	68.4	20.95	1.35	0.8†	148	89
WD2259-465	22:59:06.633	−46:27:58.86	0.414 ± 0.032	112.4	20.37	1.31	0.8†	140	71
WD0340-330	03:40:08.673	−33:01:00.30	0.606 ± 0.069	128.0	20.56	1.55	0.42	168	58
LHS 1402‡	02:24:32.255	−28:54:59.36	0.490 ± 0.030	92.6	18.32	0.46	−0.63	176	76
LHS 1274*	01:39:14.380	−33:49:03.31	0.579 ± 0.037	93.4	17.71	0.52	0.34	147	53
WD0214-419	02:14:14.887	−41:51:09.04	0.334 ± 0.026	106.7	20.63	1.17	0.48	150	95
WD0044-284	00:44:02.188	−28:24:11.15	0.348 ± 0.063	191.1	20.83	1.48	0.55	119	72
WD2214-390*	22:14:34.727	−38:59:07.05	1.056 ± 0.013	110.1	16.57	0.75	0.40	120	24
WD2324-595*	23:24:10.165	−59:28:07.95	0.581 ± 0.016	167.1	17.13	0.23	0.05	159	58
LP 588-37*	01:42:20.770	−01:23:51.38	0.354 ± 0.010	162.8	18.62	0.19	0.0†	202	120
WD0345-362	03:45:32.711	−36:11:03.60	0.589 ± 0.081	167.8	21.12	1.81	0.60	155	55
WD0045-061	00:45:06.325	−06:08:19.65	0.699 ± 0.017	171.2	18.82	1.12	0.66	145	44
WD0225-326	02:25:28.681	−32:37:53.92	0.338 ± 0.033	59.7	18.94	0.58	0.13	140	88
WD2348-548	23:48:46.904	−54:45:46.21	0.388 ± 0.033	105.5	19.76	1.14	0.51	121	66
WD0117-268	01:17:51.649	−26:48:51.21	0.468 ± 0.032	82.2	19.91	1.34	0.58	122	55
LP 651-74*	03:07:14.113	−07:14:59.12	0.477 ± 0.036	203.8	17.56	0.94	0.4†	68	30
WD0135-546	01:35:38.677	−54:35:27.78	0.675 ± 0.018	80.9	19.52	1.47	0.43	127	39
WD0100-567*	01:00:43.076	−56:46:36.61	0.414 ± 0.043	45.1	17.85	0.63	0.4†	98	50

*These stars have Hα features. All others have featureless spectra. †These *R59F* − I_N colors are calculated from spectrophotometry. ‡This object is extremely cool but has a spectrum similar to the peculiar LHS 3250 (*7*).

space density of all 38 of the halo white dwarfs in our survey, we used the $1/V_{max}$ technique (*27*), which determines the maximum volume, V_{max}, in which the survey could have found each star, given the brightness detection limit. The sum of $1/V_{max}$ for all of the stars in the sample is the number density. Because our survey was limited to stars brighter than $R59F_{lim} = 19.8$, we have computed V_{max} using the absolute *R59F* magnitudes, M_{R59F}, implied by the distances inferred above.

$$V_{max} = (4/3)\pi d_{max}{}^3\Omega/(4\pi)\mathrm{pc}^3 \quad (1)$$

Here, Ω is the surveyed area in steradians, and d_{max}, the maximum distance in parsecs (pc) that determines V_{max}, is the minimum of the two following relations

$$\log d_{max}(\mathrm{pc}) = 0.2(R59F_{lim} - M_{R59F}) + 1 \quad (2)$$

$$d_{max}(\mathrm{pc}) = d\mu/0.33 \quad (3)$$

The number density derived in this manner is 1.8×10^{-4} pc^{-3}. Using 0.6 $M_\odot$ as the average white dwarf mass in the halo (*28*), the local space density of halo white dwarfs is 1.1×10^{-4} $M_\odot$ pc^{-3}. However, our survey is not complete to the *R59F* = 19.8 level. A measure of the uniformity of our sample is given by the average value of V/V_{max} for the sample, where V is the volume of space given by the distance to the given star and the survey area. In the case of this survey, the average of V/V_{max} is 0.46. For a sample distributed uniformly in space, this value should be 0.5. An average of $V/V_{max} = 0.5$ is found for $R59F_{lim} = 19.7$, indicating that all stars brighter than 19.7 were found in the survey. Recalculating the space density using $R59F_{lim} = 19.7$ yields 1.3×10^{-4} $M_\odot$ pc^{-3}.

The density of white dwarfs in the halo predicted from the subdwarf star counts and a standard initial mass function is 1.3×10^{-5} $M_\odot$ pc^{-3} (*29*), which is 10 times smaller than the value we calculate. This means that star formation in the early galaxy must have favored higher-mass stars that would evolve into the white dwarfs we are detecting now. At the same time, this early star formation must have underproduced the low-mass subdwarfs relative to the more recent star formation processes observed in the disk (*4*).

The estimated density of halo dark matter near the sun is approximately 8×10^{-3} $M_\odot$ pc^{-3} (*30*). Thus, the population we have detected accounts for about 2% of the local dark matter. We treat this number as a lower limit for the reasons discussed above and because it appears that we have not probed the entire range of intrinsic luminosities of these objects. Indeed, the number density as a function of M_{R59F} suggests that we are only detecting the rising power law of the luminosity function and have not seen any indication of the expected turnover due to the finite lifetime of the halo white dwarf population (*31*). This means that there may be an undetected, larger population of even fainter and cooler white dwarfs in the halo.

Discussion. Microlensing experiments have indirectly revealed a population of massive, compact objects in the line of sight to the Large Magellanic Cloud. The Massive Compact Halo Object project (MACHO) (*1*) estimates that these compact objects contribute between 8 and 50% of the local halo dark matter at the 95% confidence level, and the inferred lens mass suggests that they are white dwarfs. The similar Expérience pour la Recherche d'Objets Sombres project (EROS) places a strong upper limit of 35% for such objects (*32*). Because the halo white dwarf space density that we derive from our survey represents a lower limit and is consistent with the two measurements mentioned above, the population of white dwarfs with halo kinematics that we have discovered provides a natural explanation for the microlensing results.

A number of the white dwarfs revealed in this survey may be cooler than any other white dwarf previously known. There are at least three objects (Table 1) that are comparable in temperature to WD0346+246 (*7*), representing a doubling of the number of ultracool white dwarfs known. The nature of cool white dwarfs can be discussed on the basis of their positions in color-color diagrams. Although a combination of optical and infrared colors is necessary at these low effective temperatures (*7, 23*), for now, we must contend with the limited spectral coverage of photographic plates for this sample. The comparison of B_J, *R59F*, and I_N (a bandpass centered on 0.8 μm) colors is a poor diagnostic of atmospheric composition for effective temperatures, T_{eff}, greater than 3500 K (Fig. 3). Given the large photometric error bars, there is little that distinguishes the colors of these stars from a sample of cool white dwarfs with disk kinematics (*33*).

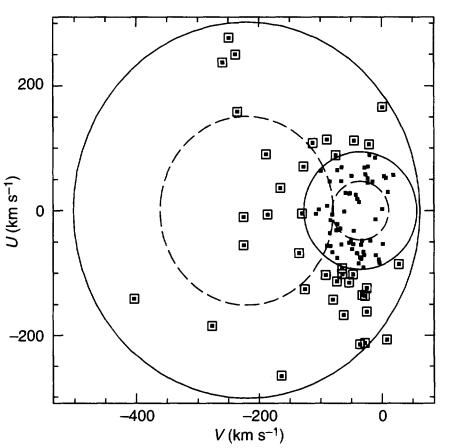

Fig. 3. Velocities of white dwarfs in the survey. The terms *U* and *V* are the galactic radial and rotational velocities, respectively, of the white dwarfs in our survey. Objects that appear in Table 1 are surrounded by boxes. The dashed ellipses indicate the velocity dispersions of the galaxy's old disk (right) and halo (left). The solid ellipses are the 2σ dispersions for these populations. The ellipses representing the old disk stars, the highest velocity members of the galaxy's disk, are centered at (*V*,*U*) = (−35,0), because this population of stars rotates slightly slower than the local standard of rest.

Stars with $B_J - R59F \lesssim 1.2$ are relatively warm, with $T_{eff} \gtrsim 5000$ K (except for the strange stars LHS 3250, SDSS 1337+00 and LHS 1402). They are also the most luminous and most distant stars in the sample (Table 1). Although it is not possible to guess the atmospheric composition of any of these stars from the present data, we point out that the sample may contain a few unusual objects, in addition to the peculiar LHS 1402 and WD2356-209 (Fig. 2B). Other inferences, however, can be made from the photographic color-color diagram (Fig. 4), using stars previously studied. LHS 542 has a pure He atmosphere and T_{eff} = 4747 K (*24*). WD0346+246 and F351-50 are similar to each other with predominantly He atmospheres, a very small admixture of H, and T_{eff} of ~3750 K and ~3500 K, respectively (*7*). The most extreme star of the sample, and also the faintest, is WD0351-564 with $B_J - R59F = 1.98$. The stars with $B_J - R59F > 1.6$ (WD0351-564, WD0205-053, and WD0345-362) may have either pure He atmospheres with $T_{eff} > 4000$ K or, more interestingly, be other examples of very cool white dwarfs with He atmospheres polluted by a small amount of H, like WD0346+246. The stars most likely to have pure H atmospheres residing below the color turn-off due to strong H_2 collision-induced opacity are WD0135-546, WD0340-330, and, perhaps, WD0351-564.

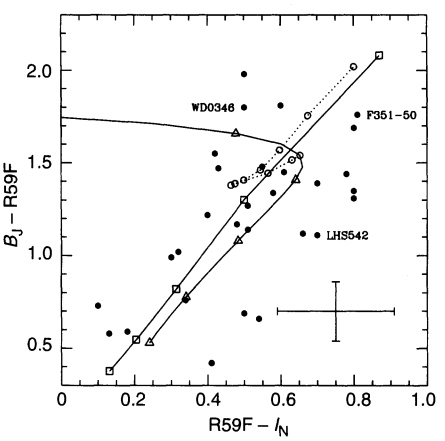

Fig. 4. Photographic color-color diagram. The cooler stars listed in 1 are shown as solid dots, and a typical error bar is indicated. The synthetic colors of pure He atmospheres (open squares) (*9*) form a diagonal sequence from T_{eff} = 8000 K (lower left) to 4000 K, in steps of 1000 K. For pure H atmospheres (open triangles) (*9*), the sequence starts at 7000 K (lower left) and turns over to bluer $R59F - I_N$ below 3500 K due to the onset of H_2 collision-induced opacity. The dotted line connecting open circles shows the effect of mixed H/He composition on a T_{eff} = 3500 K model, with the number ratio of He to H ranging from 0 to 10^7 (*7*). All models have log*g* (cm s^{-2}) = 8. As a basis for comparison, three stars whose spectra have been studied in greater detail (*3, 7*) are labeled. WD0346+246 is not part of our survey and is shown here for comparison.

We still do not understand the nature of the three strange objects LHS 3250, LHS 1402, and SDSS 1337+00 (*5–7*), all of which lie at $R59F - I_N$ colors near −0.5 (well outside of Fig. 4). The kinematics of these stars, with the exception of LHS 1402, suggest that they may be disk objects. Although they are certainly cool white dwarfs, we know neither their effective temperatures nor their atmospheric compositions. They may represent another, perhaps unusual, stage in the spectral evolution of cool white dwarfs.

The direct detection of a significant white dwarf halo population opens promising avenues of investigation. Besides the opportunity to study individual white dwarfs that are older and cooler than any known so far, dedicated studies of this population of stellar remnants will bear directly on the ancient history of the galaxy. For instance, a determination of the luminosity function of halo white dwarfs and a characterization of the low luminosity cutoff will reveal the age of the first generation of halo stars, lead to a determination of its initial mass function, and provide strong constraints on formation scenarios of the galaxy. The interpretation of observations of young galaxies at high redshifts will benefit from a better understanding of the early history of our galaxy. Finally, the complete characterization of this new stellar population will reveal whether it is responsible for the microlensing.

Note added after online publication: This text reflects the correction of a few typographical errors in the online version of the table. It also includes the new constraint on the calculation of d_{max} which accounts for the fact that the survey could not have detected stars with proper motions below 0.33 arc seconds per year.

References and Notes

1. C. Alcock *et al.*, *Astrophys. J.* **542**, 281 (2000).
2. S. T. Hodgkin *et al.*, *Nature* **403**, 57 (2000).
3. R. Ibata, M. J. Irwin, O. Bienaymé, R. Scholz, J. Guibert, *Astrophys. J. Lett.* **532**, L41 (2000).
4. G. Chabrier, *Astrophys. J. Lett.* **513**, L103 (1999).
5. H. C. Harris *et al.*, *Astrophys. J.* **524**, 1000 (1999).
6. H. C. Harris *et al.*, *Astrophys. J. Lett.* **549**, L109 (2001).
7. B. R. Oppenheimer *et al.*, *Astrophys. J.*, **550**, 448 (2001).
8. B. Hansen, *Nature* **394**, 860 (1998).
9. P. Bergeron, D. Saumon, F. Wesemael, *Astrophys. J.* **443**, 764 (1995); D. Saumon, S. Jacobson, *Astrophys. J. Lett.* **511**, L107 (1999).
10. B. Hansen, *Astrophys. J.* **520**, 680 (1999).
11. A. Borysow, L. Frommhold, *Astrophys. J. Lett.* **348**, L41 (1990).
12. N. C. Hambly *et al.*, in preparation.
13. N. C. Hambly, M. J. Irwin, H. T. MacGillivray, in preparation.
14. N. C. Hambly, A. C. Davenhall, M. J. Irwin, H. T. MacGillivray, in preparation.
15. N. C. Hambly, in *The 12th European Conference on White Dwarfs*, Newark, DE, 12 to 15 July 2000, H. Shipman, J. Provencal, Eds. (Astronomical Society of the Pacific, San Francisco, CA), in press.
16. D. G. Monet *et al.*, *Astron. J.* **120**, 1541 (2000).
17. W. J. Luyten, *NLTT Catalog* (Univ. of Minnesota Press, Minneapolis, MN, 1979).
18. R. A. Knox, M. R. S. Hawkins, N. C. Hambly, *Mon. Not. R. Astron. Soc.* **306**, 736 (1999).
19. C. Flynn, J. Sommer-Larsen, B. Fuchs, D. S. Graff, *Mon. Not. R. Astron. Soc.* **322**, 553 (2001).
20. R. D. Scholz, M. J. Irwin, R. Ibata, H. Jahreiß, O. Yu. Malkov, *Astron. Astrophys.* **353**, 958 (2000).
21. N. C. Hambly, S. J. Smartt, S. T. Hodgkin, *Astrophys. J. Lett.* **489**, L157 (1997).
22. N. C. Hambly *et al.*, *Mon. Not. R. Astron. Soc.* **309**, L33 (1999).
23. P. Bergeron, M.-T. Ruiz, S. K. Leggett, *Astrophys. J. Suppl. Ser.* **108**, 339 (1997).
24. S. K. Leggett, M.-T. Ruiz, P. Bergeron, *Astrophys. J. Lett.* **497**, L294 (1998).
25. M. Chiba, T. C. Beers, *Astron. J.* **119**, 2843 (2000).
26. P. F. L. Maxted, P. R. Marsh, *Mon. Not. R. Astron. Soc.* **307**, 122 (1999).
27. M. A. Wood, T. D. Oswalt, *Astrophys. J.* **497**, 870 (1998).
28. P. Bergeron, R. A. Saffer, J. Liebert, *Astrophys. J.* **394**, 228 (1992).
29. A. Gould, C. Flynn, J. N. Bahcall, *Astrophys. J.* **503**, 798 (1998).
30. E. I. Gates, G. Gyuk, M. S. Turner, *Astrophys. J. Lett.* **449**, L123 (1995).
31. G. Fontaine, P. Brassard, P. Bergeron, *Publ. Astron. Soc. Pac.* **113**, 409 (2001). See also C. M. Tamanaha, J. Silk, M. A. Wood, D. E. Winget, *Astrophys. J.* **358**, 164 (1990).
32. T. Lasserre *et al.*, *Astron. Astrophys.* **355**, L39 (2000).
33. P. Bergeron, S. K. Leggett, M.-T. Ruiz, *Astrophys. J.*, in press.

34. We thank M. Irwin, I. King, G. Chabrier, T. Nakajima for helpful discussions. B.R.O. is supported by a Hubble Postdoctoral Research Fellowship, grant number HF-01122.01-99A. D.S. acknowledges support from NSF Grant AST97-31438.

16 February 2001; accepted 13 March 2001
Published online 22 March 2001;
10.1126/science.1059954
Include this information when citing this paper.

REPORTS

Energy Gaps in "Metallic" Single-Walled Carbon Nanotubes

Min Ouyang,[1] Jin-Lin Huang,[1] Chin Li Cheung,[1] Charles M. Lieber[1,2]*

Metallic single-walled carbon nanotubes have been proposed to be good one-dimensional conductors. However, the finite curvature of the graphene sheet that forms the nanotubes and the broken symmetry due to the local environment may modify their electronic properties. We used low-temperature atomically resolved scanning tunneling microscopy to investigate zigzag and armchair nanotubes, both thought to be metallic. "Metallic" zigzag nanotubes were found to have energy gaps with magnitudes that depend inversely on the square of the tube radius, whereas isolated armchair tubes do not have energy gaps. Additionally, armchair nanotubes packed in bundles have pseudogaps, which exhibit an inverse dependence on tube radius. These observed energy gaps suggest that most "metallic" single-walled nanotubes are not true metals, and they have implications for our understanding of the electronic properties and potential applications of carbon nanotubes.

Are "metallic" single-walled carbon nanotubes (SWNTs) true metals (*1*)? This question has attracted theoretical interest (*2–13*) and is of increasing practical importance because of the potential applications of SWNTs in nanoelectronic devices (*14, 15*). Tight-binding calculations carried out for the two-dimensional (2D) graphene sheet model predict that SWNTs with indices $(n, n+3q)$ (where q is an integer) should behave as metallic quantum wires with high electrical conductivity (*2–4, 15*). However, the finite curvature of SWNTs alters the overlap of π-electron wave functions, and this could produce small energy gaps in "metallic" zigzag $(n,0)$ (where n is a multiple of 3) and chiral SWNTs at the Fermi energy (E_F) (*3–8*). In addition, intertube interactions can break the rotational symmetry of armchair SWNTs (n,n), which allows mixing of π and π* bands, and has been predicted to lead to a pseudogap at E_F (*9–13*).

Direct experimental data addressing these predictions have been lacking, although the nature of nanotube electronic density of states (DOS) near E_F is clearly critical to our understanding of electrical transport through these materials. We have used low-temperature scanning tunneling microscopy (STM) to characterize the atomic structure and local DOS of metallic zigzag and armchair SWNTs. The STM

[1]Department of Chemistry and Chemical Biology, [2]Division of Engineering and Applied Sciences, Harvard University, Cambridge, MA 02138, USA.

*To whom correspondence should be addressed. E-mail: cml@cmliris.harvard.edu